Journal of Dispersion Science and Technology, 34:516–527, 2013

ISSN: 0193-2691 print/1532-2351 online
DOI: 10.1080/01932691.2012.682008

Corrosion Inhibiting Effect of *Aframomum melegueta* Extracts and Adsorption Characteristics of the Active Constituents on Mild Steel in Acidic Media

E. E. Oguzie,[1] Z. O. Iheabunike,[1] K. L. Oguzie,[2] C. E. Ogukwe,[1] M. A. Chidiebere,[1] C. K. Enenebeaku,[1] and C. O. Akalezi[1]

[1]*Electrochemistry and Materials Science Research Laboratory, Department of Chemistry, Federal University of Technology Owerri, Owerri, Nigeria*
[2]*Department of Environmental Technology, Federal University of Technology Owerri, Owerri, Nigeria*

GRAPHICAL ABSTRACT

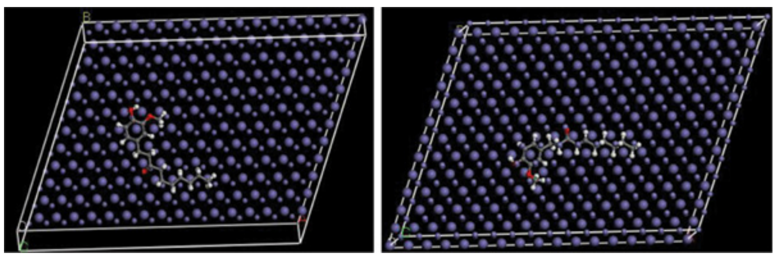

The extract from the seeds of *Aframomum melegueta* (AM) was investigated as corrosion inhibitor for mild steel in aerated 1 M HCl and 0.5 M H_2SO_4 solutions using gravimetric and electrochemical techniques. AM extract was found to inhibit both the cathodic and anodic partial reactions of the corrosion process, via adsorption of the organic matter on the metal/solution interface, as described by the Langmuir as well as Flory-Huggins adsorption isotherms. Corrosion rates in all systems studied increased with rise in temperature. Increasing the temperature of the system enhanced inhibition efficiency of AM extract in 1 M HCl, but decreased efficiency in 0.5 M H_2SO_4. Molecular dynamics simulations were performed to theoretically illustrate the electronic structure and adsorption behaviour of the active constituents of the seeds of *Aframomum melegueta*; paradol (1-(4-Hydroxy-3-methoxyphenyl)decan-3-one) and shogaol ((*E*)-1-(4-Hydroxy-3- methoxyphenyl)dec-4-en-3-one) in order to theoretically evaluate their contributions to the corrosion inhibiting action of the extract.

Keywords *Aframomum melegueta*, corrosion inhibition, inhibition efficiency, mild steel, molecular modeling

1. INTRODUCTION

Several classes of organic compounds, particularly those containing polar functions with nitrogen, oxygen or sulfur in a conjugated system, have been reported to exert inhibiting effects on the corrosion of mild steel in acidic environments.[1–6] Such substances retard the corrosion reaction via adsorption on to the metal surface, with the polar group acting as the reaction centre for the adsorption process; the resulting adsorption layer functions as a barrier, isolating the metal from the acid corrodent. The adsorbed inhibitor, depending on its molecular structure and the nature of the acid solution, may function by geometric blocking of active sites on the metal surface or may polarize the individual metal atoms to which they are attached, influencing the intrinsic reactivity of the metal. In any case, the active corrosion sites on the metal surface are occupied by the adsorbed inhibitor and the effectiveness of inhibition will be determined by the energy released on forming the metal-inhibitor bond compared to the corresponding changes when the pure acid reacts with the metal.

Received 4 March 2012; accepted 12 March 2012.

This project is supported by TWAS, the Academy of Sciences for the developing World, under the TWAS Grants for Research Units in Developing Countries Program (TWAS-RGA08-005) and the Education Trust Fund (ETF); under batch one of ETF 2009/2010 research projects intervention for the Federal University of Technology Owerri.

Address correspondence to E. E. Oguzie, Electrochemistry and Materials Science Research Laboratory, Department of Chemistry, Federal University of Technology Owerri, PMB 1526 Owerri, Nigeria. E-mail: oguziemeka@yahoo.com or emekaoguzie@gmail.com

Despite the wide availability of organic compounds that could function as corrosion inhibitors, the final choice of an appropriate inhibitor for a particular application is restricted by a number of factors, including the costs and known hazard effects of most synthetic corrosion inhibitors. Again, the corrosion of a given piece of iron often proceeds via dissimilar reaction routes in different environments, which means that a substance may be required to perform more than one function in order to be an effective corrosion inhibitor. On the other hand, acid inhibitors are often quite specific in action; hence, combinations of inhibitors are often required in order to provide the multiple services required for effective corrosion inhibition. The above challenges provide sufficient motivation for the development of new classes of corrosion inhibitors that are inexpensive, non toxic and all-round effective.

The exploration of natural products of plant origin as inexpensive eco-friendly corrosion inhibitors is becoming an important field of study.[7–12] The extracts from the leaves, barks, seeds, fruits and roots of such plants contain organic constituents with molecular structures containing nitrogen or oxygen atoms and could have considerable potential as inexpensive, non toxic, readily available and renewable sources of corrosion inhibiting additives. Again, the complex composition of biomass extracts, should overcome the restrictions inherent in the specificity of action of single compounds as the mixtures of organic compounds therein may possibly provide the multiple services required for effective corrosion inhibition.

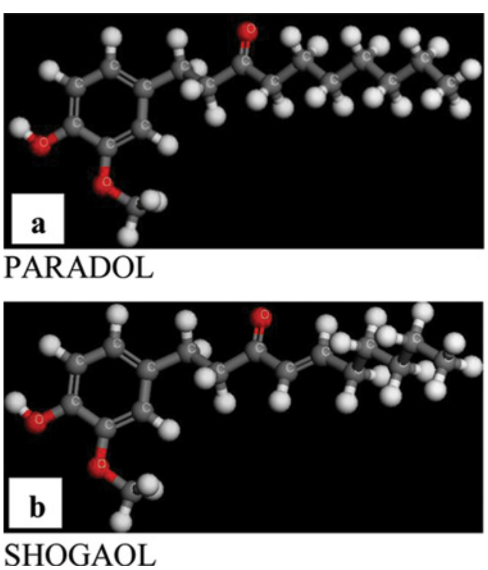

FIG. 1. Molecular structures of the active constituents of *Aframomum melegueta* (AM); (a) 1-(4-hydroxy-3-methoxyphenyl) decan-3-one (paradol) and (b) (*E*)-1-(4-hydroxy-3- methoxyphenyl)dec-4-en-3-one (shogaol). (Figure available in color online.)

This article reports on the corrosion inhibiting efficacy of extracts from the seeds of *Aframomum melegueta* (AM) on mild steel corrosion in hydrochloric and sulfuric acid solutions. *Aframomum melegueta* (Guinea pepper, melegueta pepper, alligator pepper and Guinea grains) is a species in the ginger family, Zingiberaceae. It is an herbaceous perennial plant native to the West African coast and used in traditional medicine as a remedy for variety of ailments such as stomach ache and snakebite.[13] Paradol (1-(4-Hydroxy-3-methoxyphenyl)decan-3-one) (Figure 1a) and shogaol ((*E*)-1-(4-Hydroxy-3-methoxyphenyl)dec-4-en-3-one) (Figure 1b) are the known active flavor (pungent) constituents of the seeds of *Aframomum melegueta*.[14,15] Interestingly, the molecular structures of both molecules bear close similarities with those of conventional organic corrosion inhibitors. We have thus also undertaken theoretical assessment of structural and electronic properties of both paradol and shogaol, including molecular dynamics simulation of their interactions with a metal surface, within the framework of the density functional theory (DFT).

2. EXPERIMENTAL

2.1. Materials Preparation

Tests were performed on carbon steel specimens with weight percentage composition as follows; C–0.05; Mn–0.6; P–0.36; Si–0.3 and the balance Fe. The blank corrodents were respectively 1.0 M HCl and 0.5 M H_2SO_4 solutions. Stock solutions of the plant extract were prepared by boiling weighed amounts of the dried and ground seeds of AM under reflux for 3 hours in 1.0 M HCl and 0.5 M H_2SO_4 solutions, respectively. The resulting solutions were cooled then triple filtered. The amount of plant material extracted into solution was quantified by comparing the weight of the dried residue with the initial weight of the dried plant material before extraction. From the respective stock solutions, inhibitor test solutions were prepared in the concentration range of 25 to 800 mg/L in respective corrodents.

2.2. Gravimetric Experiments

Gravimetric experiments were conducted on test coupons of dimension $3\,cm \times 3\,cm \times 0.14\,cm$. These coupons were used as cut without further polishing. They were however degreased in absolute ethanol, rinsed with water, dried in acetone and warm air. The pre-cleaned and weighed coupons were suspended in beakers containing the test solutions using glass hooks and rods. Tests were conducted under total immersion conditions in 300 ml of the aerated and unstirred test solutions. To determine weight loss with respect to time, the coupons were retrieved from test solutions at 3 hours intervals, appropriately cleaned, dried and re-weighed. The weight loss was taken to be the difference between the weight of the coupons at a given time and its initial weight. All tests were run in triplicate and the data showed good reproducibility. Average values for each experiment were obtained and used in subsequent calculations.

The effect of temperature on the corrosion and corrosion inhibition processes was investigated by carrying out gravimetric experiments in the temperature range of 303 to 333 K.

2.3. Electrochemical Measurements

Metal samples for electrochemical experiments were of dimensions $1.5 \times 1.5 \times 0.14$ cm. These were subsequently sealed with epoxy resin in such a way that only one square surface of area $1.0\,cm^2$ was left uncovered. The exposed surface was ground with silicon carbide abrasive paper (from grade #200 to #1000), degreased in acetone, rinsed with distilled water and dried in warm air. Electrochemical experiments were conducted in a conventional three-electrode cell using a Versastat 400 Complete DC Voltammetry and Corrosion System, with V3 Studio software. A graphite rod was used as counter electrode and a saturated calomel electrode (SCE) as reference electrode. The latter was connected via a Luggin's capillary. Measurements were performed in aerated and unstirred solutions at the end of 1 hour of immersion at 303 K. Impedance measurements were made at corrosion potentials (E_{corr}) over a frequency range of 100 kHz to 10 mHz, with a signal amplitude perturbation of 5 mV. Potentiodynamic polarization studies were carried out in the potential range $\pm$ 250 mV versus corrosion potential at a scan rate of $0.333\,mV\,s^{-1}$. Each test was run in triplicate to verify the reproducibility of the systems.

3. RESULTS AND DISCUSSION

3.1. Weight Loss and Corrosion Rate

Gravimetric measurements were undertaken in this study to assess the weight losses and hence corrosion rates of mild steel test coupons immersed in 1 M HCl and 0.5 M H_2SO_4 for a 3 hours immersion period at 303 K. The data presented are means of triplicate determinations, with standard deviation <0.001. Figure 2 shows the weight losses of mild steel coupons in 1 M HCl and 0.5 M H_2SO_4 without and with different concentrations of AM extract. The plots show higher corrosion rates in 0.5 M H_2SO_4 and as well provide clear evidence that AM extract inhibited the corrosion reaction in both acid environments, even though this effect was more pronounced in 0.5 M H_2SO_4. The inhibiting effect improves with increasing AM extract concentration, implying a dependence of the inhibition process on the amount of inhibiting species present in the system.

3.1.2. Inhibition Efficiency

The inhibition performance of AM extract on mild steel corrosion was quantified by evaluating the inhibition efficiency IE (%) as follows:

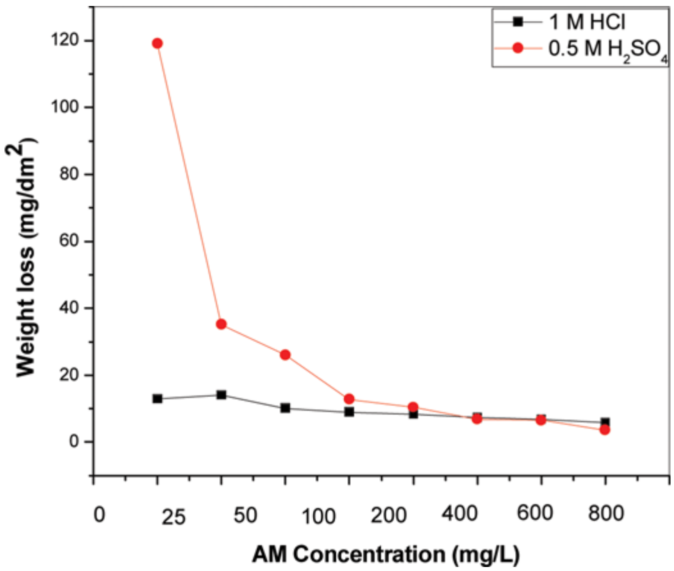

FIG. 2. Weight loss of mild steel 1 M HCl and 0.5 M H_2SO_4 without and with different concentrations of *Aframomum melegueta* (AM) extract at 30°C. (Figure available in color online.)

$$IE\ \% = \left(1 - \frac{\Delta W_{inh}}{\Delta W_{blank}}\right) \times 100, \quad [1]$$

where ΔW_{inh} and ΔW_{blank} represent the weight losses in inhibited and uninhibited solution, respectively. The trend of IE (%) with AM extract concentration in 0.5 M H_2SO_4 and 1 M HCl is illustrated in Figure 3 and shows that inhibition efficiency increased with AM extract concentration reaching maximum values of 55% and 96.1% in 1 M HCl and 0.5 M H_2SO_4, respectively.

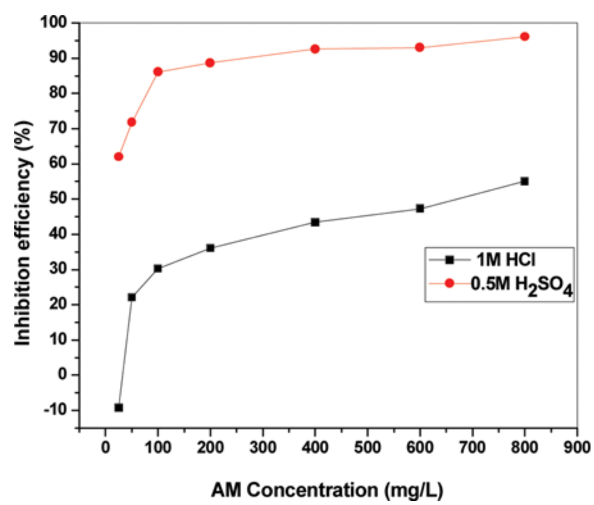

FIG. 3. Trend of inhibition efficiency with concentration of AM extract for mild steel corrosion in 1 M HCl and 0.5 M H_2SO_4 at 30°C. (Figure available in color online.)

3.2. Electrochemical Measurements

The corrosion reaction is an electrochemical process and as such electrochemical measurements are most appropriate for obtaining in-depth mechanistic insights into corrosion systems. Tests to ascertain the influence of low and high concentrations of AM extract on the electrochemical corrosion behavior of mild steel in 1 M HCl and 0.5 M H_2SO_4 were thus carried out using 50 mg/L and 800 mg/L concentrations of AM.

3.2.1. Potentiodynamic Polarization

Potentiodynamic polarization experiments were carried out to understudy the influence of AM extract on the kinetics of the anodic ($Fe \rightarrow Fe^{2+} + 2e$) and cathodic partial reactions ($2H^+ + 2e \rightarrow H_2$) of the corrosion process. Figures 4a and 4b show typical potentiodynamic polarization curves for the mild steel specimens in 1 M HCl and 0.5 M H_2SO_4 respectively, without and with AM extract. The corresponding electrochemical parameters derived from the polarization experiments are presented in Table 1. The mild steel specimen is seen to exhibit active dissolution with no distinctive transition to passivation within the studied potential range in all environments. The polarization curves in Figure 4 show that addition of AM extract in either acid environment did not notably alter the corrosion potentials and inhibited both the anodic and cathodic partial reactions of the corrosion process. This implies that AM extract functioned therein as a mixed-type inhibitor, reducing the rates of both anodic and cathodic reactions.

The values of the corrosion current density in the absence ($i_{corr,bl}$) and presence of inhibitor ($i_{corr,inh}$) were used to estimate the inhibition efficiency from polarization data ($IE_i\%$) as follows:

$$IE_i\,\% = \left(1 - \frac{i_{corr,inh}}{i_{corr,bl}}\right) \times 100 \quad [2]$$

The obtained values (Table 1), although different from those obtained from gravimetric measurements, however follow the same trend.

3.2.2. Electrochemical Impedance Spectroscopy

Impedance studies were undertaken to provide insight into the kinetics of electrode processes at the Fe/1 M HCl and Fe/0.5 M H_2SO_4 interfaces in absence and presence of AM extract. The impedance responses of these systems are given in Figures 5a and 5b, respectively, in the Nyquist format. The plots generally comprise of only one depressed capacitive semicircle in the high frequency region. The observed depression of the Nyquist semicircle with center under the real axis is typical for solid metal electrodes that show frequency dispersion of the impedance data.[16,17] The transfer function can be represented by a solution resistance R_s, shorted by a capacitor (C) that is placed in parallel to the charge transfer resistance R_{ct}:

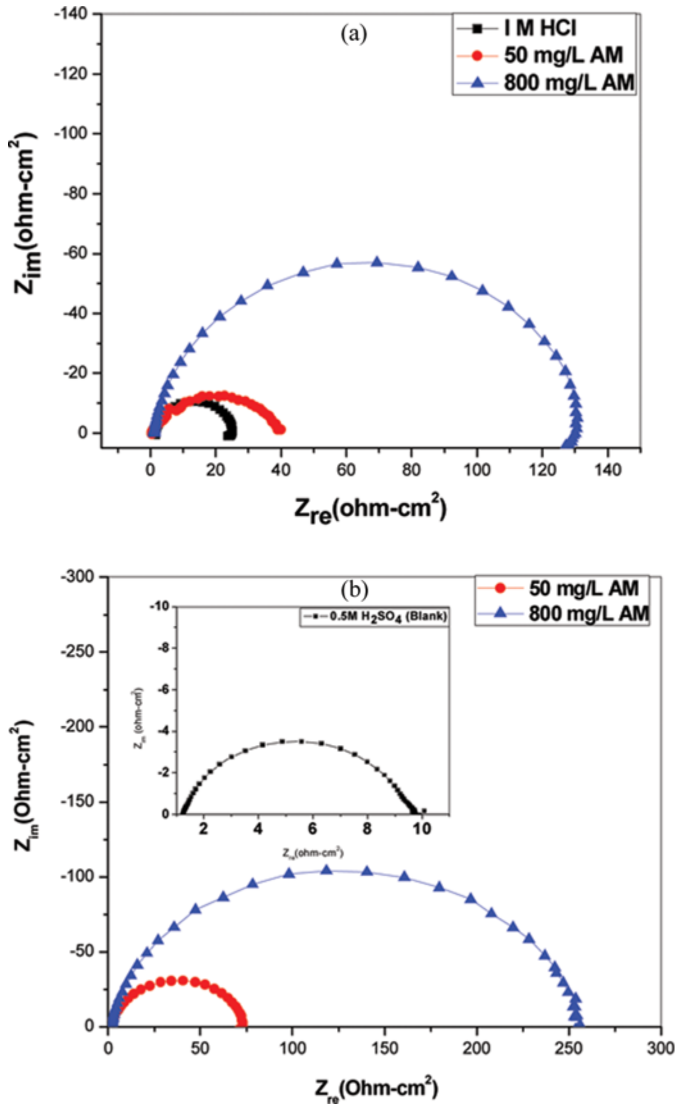

FIG. 4. Electrochemical impedance spectra of mild steel in (a) 1 M HCl solution and (b) 0.5 M H_2SO_4 without and with AM extract. (Figure available in color online.)

$$Z_{(\omega)} = R_s + \left(\frac{1}{R_{ct}} + j\omega C\right)^{-1}. \quad [3]$$

This transfer function is however only applicable for homogeneous systems and cannot account for the depression of the capacitive semicircle. In the case of a non ideal frequency response, the capacitor is replaced by a constant phase element (CPE) to account for the deviations from ideal dielectric behavior. The impedance, Z of the CPE

TABLE 1
Electrochemical parameters for mild steel in 1 M HCl and 0.5 M H_2SO_4 without and with AM extract

System	E_{corr} (mV) vs. SCE	i_{corr} ($\mu A/cm^2$)	IE_i (%)	$Q_{dl} \times 10^{-6}$ ($\mu\Omega^{-1} S^n cm^{-2}$)	R_{ct} (Ω-cm^2)	IE_R (%)
1 M HCl (blank)	−508	3253	—	218	23.5	—
50 mg/L AM	−502	1914.5	41.1	163.8	38.6	39.1
800 mg/L AM	−506	634.4	80.5	79.5	129.7	81.9
0.5 M H_2SO_4 (bank)	−503	4968	—	346	9.79	—
50 mg/L AM	−486	1172.6	76.4	105.2	67.8	85.5
800 mg/L AM	−458	193.4	96.1	86.7	274.1	96.4

corresponds to:

$$Z_{CPE} = Q_{dl}^{-1}(j\omega)^{-n}, \quad [4]$$

where Q_{dl} and n stand for the CPE constant and exponent respectively, $j = (-1)^{1/2}$ is an imaginary number, ω is the angular frequency in rad s^{-1}, ($\omega = 2\pi f$) where f is the frequency in Hz. The impedance spectra for the Nyquist plots were appropriately analyzed by fitting to the equivalent circuit model $R_s(Q_{dl}R_{ct})$, which has been previously used to model the Fe/acid interface.[18,19] The impedance parameters presented in Table 1 reveal that AM extract increased the magnitude of R_{ct} and decreased the Q_{dl} values. The former effect, which corresponds to an increase in the diameter of the Nyquist semicircle, is due to the corrosion inhibiting efficacy of AM extract. The latter effect can be related to the Helmholtz equation;

$$C_{dl} = \varepsilon\varepsilon_o A/\delta, \quad [5]$$

where C_{dl} is the double layer capacitance, ε is the dielectric constant of the medium, ε_o the vacuum permittivity, A the electrode area and δ the thickness of the electrical double layer. The observed decrease in Q_{dl} could be attributed to a decrease in the dielectric constant (due to replacement of adsorbed water molecules by organic matter from the extract, with smaller dielectric constant) and an increase in the double layer thickness, which suggests that organic constituents of AM extract become adsorbed on and modify the metal/electrolyte interface.

Inhibition efficiency from the impedance data (IE_R%) was estimated by comparing the values of the charge transfer resistance in the absence ($R_{ct,bl}$) and presence of inhibitor ($R_{ct,inh}$) as follows:

$$IE_R\,\% = \left(\frac{R_{ct(inh)} - R_{ct}}{R_{ct(inh)}}\right) \times 100. \quad [6]$$

The calculated values presented in Table 1 follow the same trend as those from the gravimetric and polarization results.

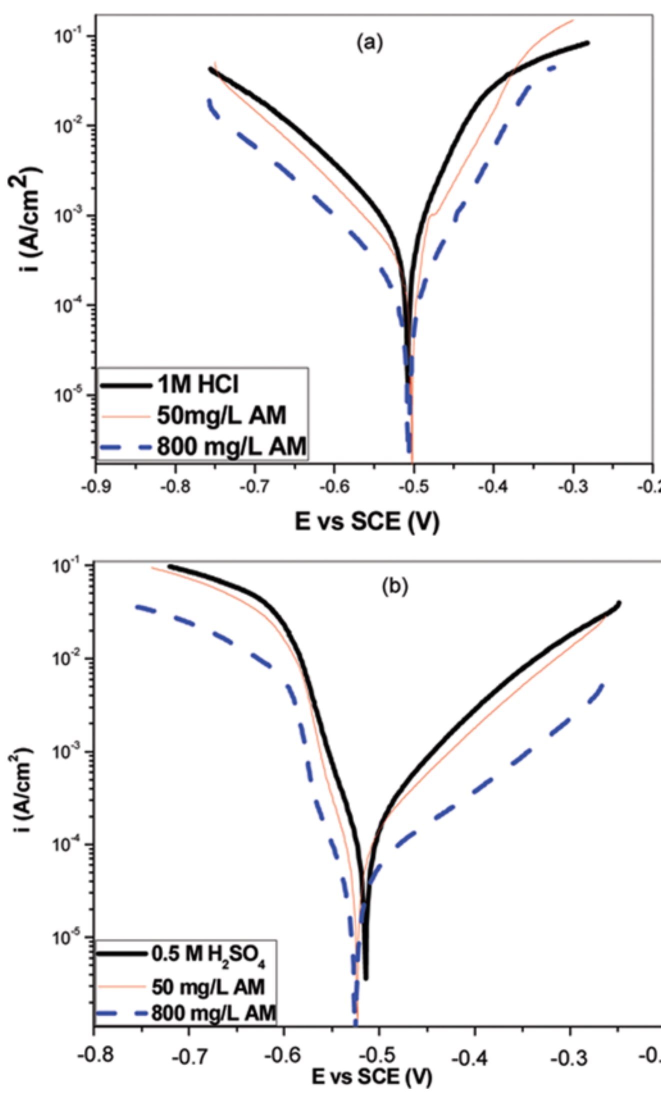

FIG. 5. Potentiodynamic polarization curves of mild steel in (a) 1 M HCl and (b) 0.5 M H_2SO_4 solution without and with AM extract. (Figure available in color online.)

3.3. Adsorption Considerations

The relationship between the degree of surface coverage, θ (related to the inhibition efficiency by IE (%) $= \theta \times 100$) and AM extract concentration was adapted to determine the adsorption characteristics of AM extract on mild steel in the different acid media in accordance with the Langmuir isotherm (Equation (7)) and the Flory-Huggins isotherm (Equation (8))[20]:

$$C/\theta = 1/b + C \quad [7]$$

$$\log(\theta/C) = \log\ K + \times \log(1 - \theta) \quad [8]$$

C is the inhibitor concentration, b is a constant, x the number of water molecules replaced by one inhibitor molecule and K is the equilibrium constant for the adsorption process. The plot of C/θ vs C is shown in Figure 6 to be linear for AM extract in both 1 M HCl (Figure 6a) and 0.5 M H_2SO_4 (Figure 6b), with slopes of 1.68 and 1.03, respectively, suggesting that the experimental data follows the Langmuir isotherm. Also, linear plots of log (θ/C) against log ($1 - \theta$) as shown in Figure 7 suggest that the adsorption of AM extract from both 1 M HCl (Figure 7a) and 0.5 M H_2SO_4 (Figure 7b), obeyed the substitution isotherm of Flory-Huggins. The fit of the gravimetric data to the two isotherms further confirms adsorption of the extract constituents on the corroding metal surface.

The deviation of the slopes of the Langmuir plots from unity can be attributed to interactions between adsorbate species on the metal surface as well as changes in the adsorption heat with increasing surface coverage.[21] The difference in the computed values of the slopes obtained in the two acid media could possibly be related to the disparity in the calculated inhibition efficiencies of AM extract in both acid solutions and probably suggests that two different mechanisms are in operation.

Some of the organic constituents of AM extract should be protonated in the acid solutions, whilst the rest remain in the molecular form. Therefore, the observed inhibiting efficiency of AM can be attributed to the participation of both protonated and molecular species in the adsorption process and the variation in inhibition efficiency of the extract in 1 M HCl and 0.5 M H_2SO_4 result from differences in the modes of adsorption in both acid solutions. The positive surface charge on mild steel in both sulfuric and hydrochloric acid solutions restricts adsorption of protonated species, due to electrostatic repulsions. On the other hand, chloride ions present in hydrochloric acid can become strongly adsorbed on the metal surface and hence facilitate adsorption of protonated species. This effect, which is not that pronounced with the sulfate ion, ensures a significant adsorption of protonated inhibitor species on the mild steel surface immersed in 1 M HCl, whereas the metal specimen immersed in 0.5 M H_2SO_4 is more predisposed to adsorption of non protonated species, yielding the observed variations in inhibition efficiency, including the marked difference in the slopes of the linear Langmuir isotherm plots.

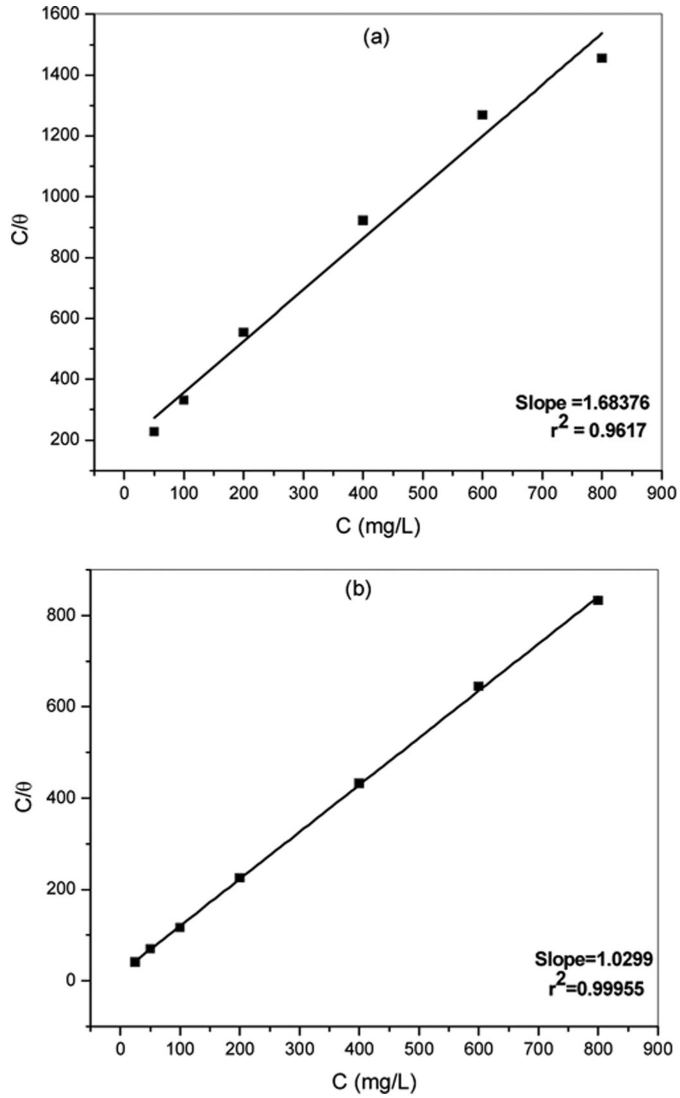

FIG. 6. Langmuir adsorption isotherm for AM extract on mild steel in (a) 1 M HCl and (b) 0.5 M H_2SO_4 solutions.

3.5. Effect of Temperature

In order to evaluate the effect of temperature variation on the corrosion and corrosion inhibition processes, gravimetric tests were further undertaken at 313–333 K in both uninhibited and inhibited systems (1 M HCl; HCl + 25 mg/L AM; HCl + 800 mg/L AM) and (0.5 M H_2SO_4; H_2SO_4 + 25 mg/L AM; H_2SO_4 + 800 mg/L AM). AM extract concentrations were selected to appropriately reflect the temperature effects at low and high surface coverage. The results obtained after a 3 hours immersion period are

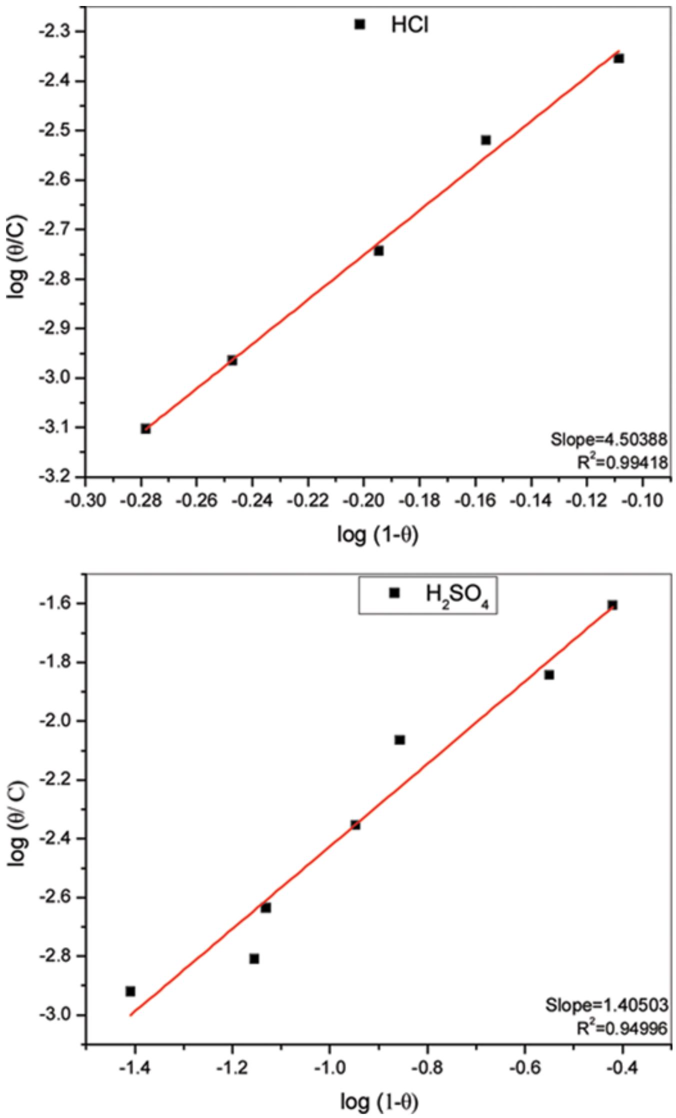

FIG. 7. Flory-Huggins adsorption isotherm for AM extract on mild steel in (a) 1 M HCl and (b) 0.5 M H_2SO_4 solutions. (Figure available in color online.)

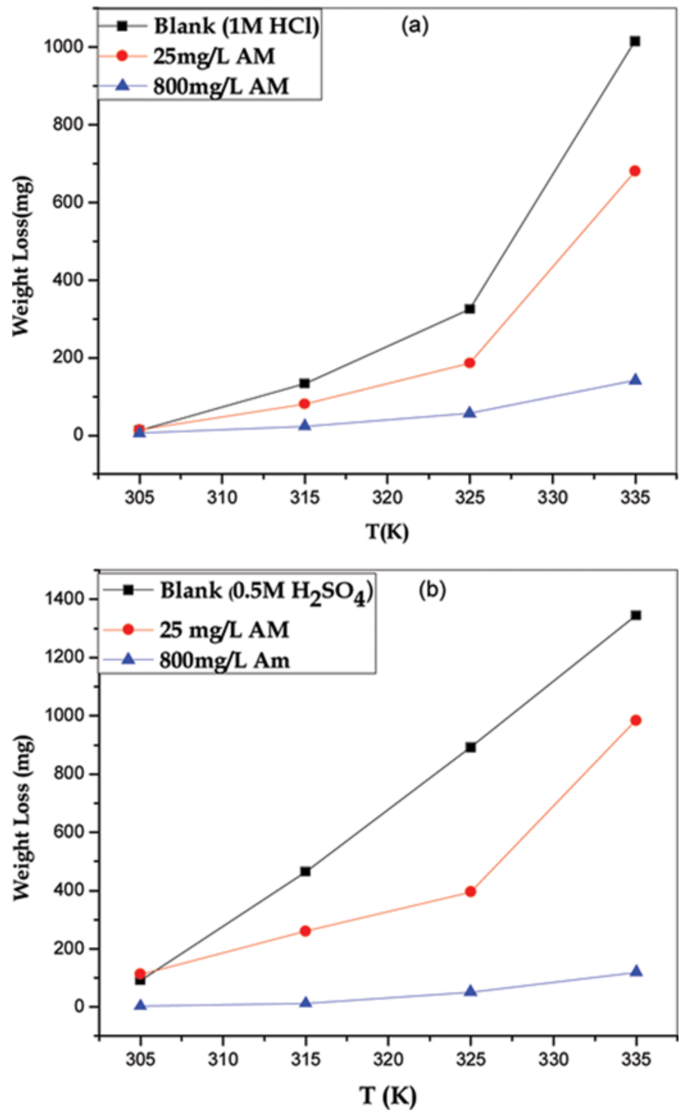

FIG. 8. Effect of temperature on the corrosion rates of mild steel (a) 1 M HCl and (b) 0.5 M H_2SO_4 solutions without and with AM. (Figure available in color online.)

presented in Figure 8 for 1 M HCl (Figure 8a) and 0.5 M H_2SO_4 (Figure 8b) and show that corrosion rates in both uninhibited and inhibited acids increased with rise in temperature. Also, AM is seen to retard the corrosion reaction at all temperatures. Figure 9 illustrates the trend of inhibition efficiency with temperature. Inhibition efficiency in 1 M HCl increased rapidly with rise in temperature at low as well as high AM concentrations (Figure 9a). This suggests that some constituents of the extract are chemically adsorbed on the mild steel surface[22,23] and exert a controlling influence on the corrosion inhibition performance of the extract. Chemisorption of such constituents is enhanced with rise in temperature, leading to greater surface coverage and hence inhibition efficiency. Inhibition efficiency in 0.5 M H_2SO_4 decreased with rise in temperature for low and high AM extract concentrations (Figure 9b). Such decrease in inhibition efficiency with rise in temperature is often attributed to physisorption of inhibitor species on the corroding metal surface.[23,24] The physisorption process is hindered by the enhanced rates of hydrogen gas evolution at higher temperatures, which increasingly agitates the interface and also promotes dispersal of adsorbed inhibitor. Accordingly, an increase in temperature is accompanied by desorption of those constituents of AM extract that are attached to the metal surface via physical adsorption, leading to reduced surface coverage, hence lower inhibition efficiency. This notwithstanding, the obtained inhibition efficiency for 800 mg/L AM exceeded

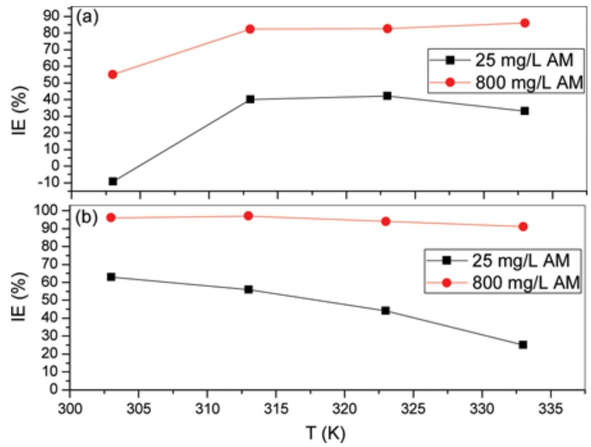

FIG. 9. Relationship between inhibition efficiency of AM extracts and temperature for mild steel corrosion in (a) 1 M HCl and (b) 0.5 M H_2SO_4 solutions. (Figure available in color online.)

90% at all temperatures, demonstrating the exceptional corrosion inhibiting properties of AM extract.

The apparent activation energies (E_a) for mild steel corrosion in 1 M HCl and 0.5 M H_2SO_4 solutions in the presence and absence of AM were evaluated from Arrhenius equation;

$$K = A \exp(-E_a/RT), \qquad [9]$$

where A is the pre-exponential factor and R; the universal gas constant. Plots showing variation of logarithm of corrosion rate (log K) with reciprocal of absolute temperature (1/T) for both acid systems are shown in Figure 10. Values of E_a obtained from the plots are presented in Table 2. Consistent with the trend of inhibition efficiency with temperature, addition of AM extract is seen to decrease E_a for the corrosion reaction in 1 M HCl, implying that the extract is more effective in this medium at high temperatures. On the other hand, AM extract increased the activation energy in 0.5 M H_2SO_4, showing that the extract herein is more effective at low temperatures.

3.4. Theoretical Considerations

Our experimental results so far show that the corrosion-inhibiting action of AM extract results from adsorption of the organic matter on the corroding mild steel surface. Such metal-inhibitor interactions have been theoretically investigated at the molecular level using computer simulations of suitable models in the framework of the DFT. We have performed such computations to model the electronic and adsorption structures of the active constituents of AM; paradol and shogaol. The motivation for the computational study is not so much as to provide in depth explanation of the adsorption of the extract, but rather to give a theoretical framework in which to recognize the relative

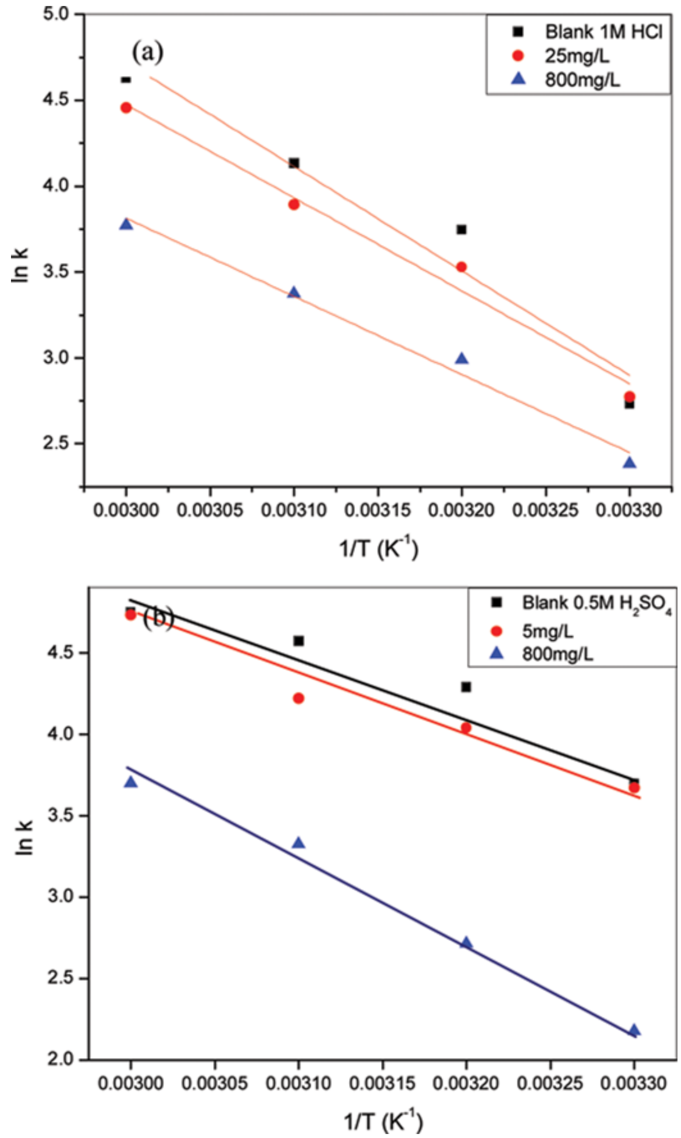

FIG. 10. Arrhenius plots for mild steel corrosion in (a) 1 M HCl and (b) 0.5 M H_2SO_4 without and with AM. (Figure available in color online.)

contributions of different extract components vis-à-vis their individual adsorption mechanisms and adsorption strengths.

TABLE 2
Corrosion activation energies (E_a) for mild steel in 1 M HCl and 0.5 M H_2SO_4 without and with AM extract

	E_a (kJ mol^{-1})	
System	1 M HCl	0.5 M H_2SO_4
Blank	50.5	28.6
25 mg/L AM	45.0	57.9
800 mg/L AM	37.8	43.4

Our computations were performed by means of the DFT electronic structure program $DMol^3$ using a Mulliken population analysis.[25,26] Electronic parameters for the simulation include restricted spin polarization using the DND basis set and the Perdew Wang (PW) local correlation density functional. Geometry optimization was achieved using COMPASS force field and the Smart minimize method by high-convergence criteria. This was followed by modeling the electronic structures of the molecules, including the distribution of frontier orbitals and Fukui indices in order to establish the active sites as well as the local reactivity of the molecules. The highest occupied molecular orbital (HOMO), lowest unoccupied molecular orbital (LUMO), Fukui functions as well as the total electron density of paradol and shogaol are presented in Figures 11 and 12, respectively, while Table 3 provides some quantum-chemical parameters related to the molecular electronic structure of the most stable conformation of the molecules.

The HOMO regions are the sites at which electrophiles attack and represent the active centers with the utmost ability to interact with the metal surface atoms, whereas the LUMO orbital can accept electrons from the metal using antibonding orbitals to form feedback bonds.[27–30] Close examination of Figures 11 and 12 reveals that the electronic distribution of both molecules are somewhat identical, which is not unexpected since their molecular structures are alike (the only difference being the presence of a double bond in the decan-3-one side chain of shogaol). The HOMO for either molecule is saturated around the methoxyphenol ring, while the LUMO density is around the carbonyl function of the decan-3-one side chain (with an extra contribution around the double bond in shogaol). For the Fukui functions, which assess reactive regions in terms of nucleophilic (f^+) and electrophilic (f^-) attack, it can be seen that the f^- functions of both molecules correspond with the HOMO locations, indicating the sites through which the molecules may be adsorbed on the metal surface, whereas f^+ correspond with the LUMO locations, showing sites through which the molecules could interact with the non bonding electrons in the metal. The electron density (charge distribution) is saturated all around each molecule; hence we should expect flat-lying adsorption orientations. A high value of the HOMO energy (E_{HOMO}) indicates the tendency of a molecule to donate electrons to an appropriate acceptor molecule with low energy or an empty electron orbital, in this case vacancies in the 3d orbital of the Fe atom. The energy of the LUMO characterizes the susceptibility of molecules towards nucleophilic attack. Low values of the energy of the gap $\Delta E = E_{LUMO\text{-}HOMO}$ implies that the energy to remove an electron from the last occupied orbital will be minimized, corresponding to improved inhibition

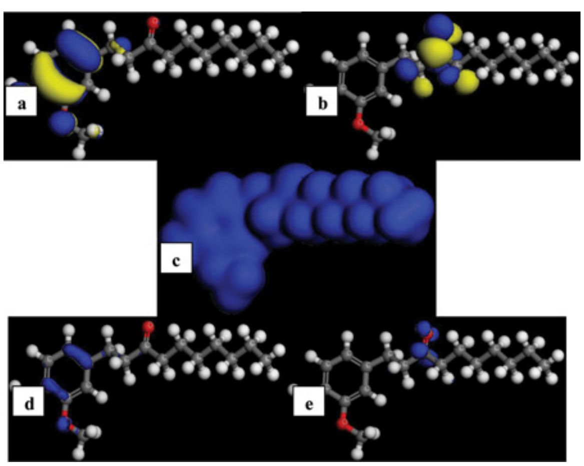

FIG. 11. Electronic properties of paradol (a) HOMO orbital; optimized structure; (b) LUMO orbital; (c) total electron density; (d) Fukui (f^-) function (e) Fukui (f^+) function. The blue and yellow isosurfaces depict the electron density difference; the blue regions show electron accumulation while the yellow regions show electron loss. (Figure available in color online.)

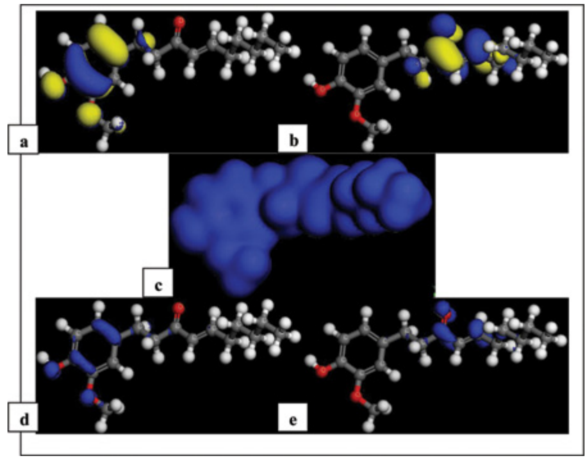

FIG. 12. Electronic properties of shogaol (a) HOMO orbital; optimized structure; (b) LUMO orbital; (c) total electron density; (d) Fukui (f^-) function (e) Fukui (f^+) function. The blue and yellow isosurfaces depict the electron density difference; the blue regions show electron accumulation while the yellow regions show electron loss. (Figure available in color online.)

TABLE 3
Calculated quantum chemical properties for the most stable conformation of selected phytochemical constituents of AM

Property	Paradol	Shogaol
E_{HOMO} (eV)	−4.90	−4.83
E_{LUMO} (eV)	−1.57	−2.41
$E_{LUMO\text{-}HOMO}$	3.33	2.42
Molecular surface area (sq. Å)	371.3	363.5

efficiencies.[29–32] As anticipated, E_{HOMO} values do not vary very significantly for paradol and shogaol, which means that any observed differences in their adsorption strengths would result from molecular size parameters rather than electronic structure parameters. The lower E_{LUMO} value of shogaol is caused by the extra contribution from the double bond in the decan-3-one side chain and suggests that the molecule would more readily undergo back-bonding interactions. The seemingly high values of ΔE ($\sim$3 eV) are in accordance with the non specific nature of the interactions of the molecules with the metal surface.

Noncovalent adsorption of the different molecules on the metal surface was modeled at a molecular level by molecular dynamics simulations to sample many different low energy configurations and identify the low energy minima. This was achieved using Forcite quench molecular dynamics in the MS Modeling 4.0 software.[33,34] The model metal surface comprised of a Fe crystal cleaved along the (110) plane, with a vacuum layer of 20 Å height. The geometry of the bottom layer of the slab was constrained to the bulk positions whereas other degrees of freedom were relaxed before optimizing the Fe (110) surface, which was subsequently enlarged into a 12×10 supercell. The adsorbate molecules were adsorbed on one side of the slab. Calculations were carried out using the COMPASS force field and the Smart algorithm. Temperature was fixed at 303 K, with NVE (microcanonical) ensemble, with a time step of 1fs and simulation time 5 ps. The system was quenched every 250 steps. Optimized structures of paradol, shogaol and the Fe surface were used for the simulation.

The lowest energy adsorption models for paradol and shogaol on the Fe (110) surface from our simulation are shown in Figures 13 and 14. The molecules can be seen to maintain a flat-lying adsorption orientation on the Fe surface as expected from the delocalization of the electron density all around the molecules. This orientation maximizes contact; hence augments the degree of surface coverage. Quantitative appraisal of the interaction between each molecule and the Fe surface was achieved by calculating the adsorption energy (E_{ads}) using the following equation:

$$E_{Bind} = E_{total} - (E_{Mol} + E_{Fe}) \qquad [10]$$

E_{mol}, E_{Fe} and E_{total} correspond, respectively, to the total energies of the molecule, Fe (110) slab and the adsorbed Mol/Fe (110) couple. In each case the potential energies were calculated by averaging the energies of the five

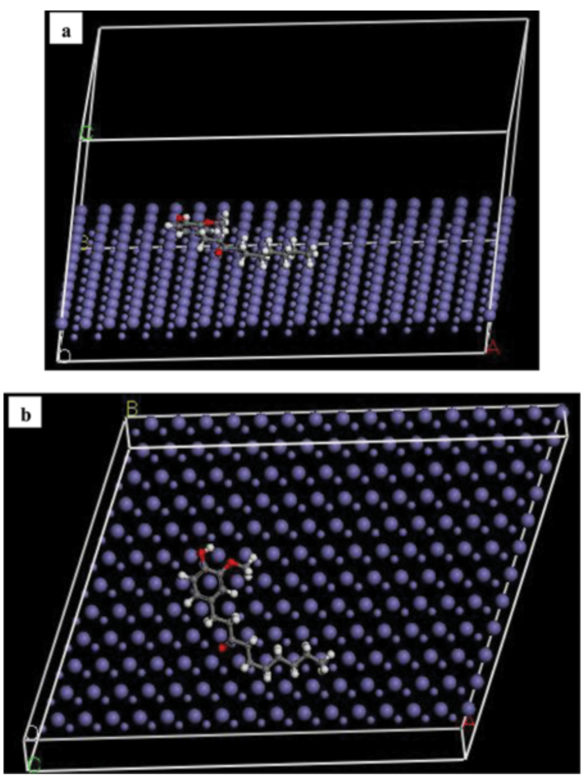

FIG. 13. Representative snapshots of paradol on Fe (110) (a) side view and (b) on-top view emphasizing the soft epitaxial adsorption mechanism with accommodation of the molecular backbone in characteristic epitaxial grooves on the metal surface (binding energy = −171.2 kcal/mol). (Figure available in color online.)

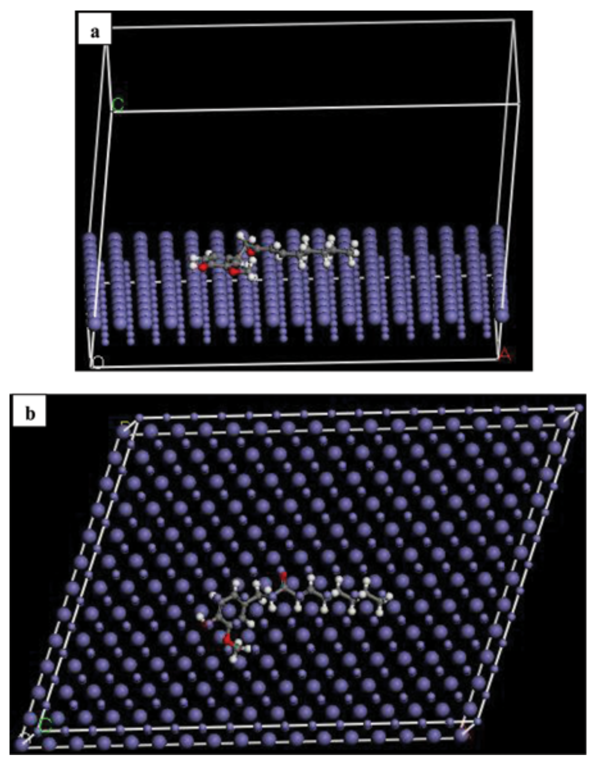

FIG. 14. Representative snapshots of shogaol on Fe (110) (a) side view and (b) on-top view emphasizing the soft epitaxial adsorption mechanism with accommodation of the molecular backbone in characteristic epitaxial grooves on the metal surface (binding energy = −168.6 kcal/mol). (Figure available in color online.)

structures of lowest energy and a negative value of E_{ads} corresponds to a stable adsorption structure. The obtained values of E_{ads} (-171.2 kcal/mol and -168.6 kcal/mol for paradol and shogaol, respectively) are of the same magnitude, which means that both molecules exert similar comparable contributions to the observed corrosion inhibiting effect of AM extract. More importantly however is the large negative values of the computed adsorption energies, which is more exothermic than expected for non covalent interactions. This probably results from significant dispersive interactions arising from the high polarizability of the O atoms and pi electron delocalization, which should enhance adsorption of the molecules. Moreover, close inspection of the on-top view of the molecules adsorbed on Fe (110) reveals a very clear trend in the adsorption configuration of both molecules wherein polarizable atoms along the molecular backbone as well as the phenyl ring align with vacant sites on the fcc lattice atop the metal surface and actually avoid contact with the Fe atoms on the surface plane (larger spheres on the Fe slab). This corresponds to accommodation of the molecular backbone in characteristic epitaxial grooves on the metal surface. Epitaxial adsorption orientations have been reported for non covalent adsorption of amino acids[35,36] as well as phytochemical constituents of certain biomass extracts on metal surfaces.[37,38] Such orientations are associated with a minimum free energy of adsorption as the adsorbed molecules can be considered as extensions of the fcc lattice and adsorption strength scales with improved fit of the polarizable atoms of a molecule to multiple epitaxial sites. This phenomenon accounts for the obtained high binding energies of the phytochemical constituents of AM, hence, the remarkable corrosion inhibiting effect of the extract as observed experimentally.

4. CONCLUSIONS

Aframomum melegueta (AM) extract effectively inhibited mild steel corrosion in 1 M HCl and 0.5 M H_2SO_4 solutions in the temperature range of 303 to 333 K. Inhibition efficiency improved with the extract concentration. Polarization measurements suggest mixed-inhibition mechanism, which the impedance data indicate was achieved via adsorption of the extract organic matter on the mild steel surface. Adsorption was further corroborated by the experimental data fit to the Langmuir and Flory-Huggins adsorption isotherms. The trend of inhibition efficiency with temperature as well as values of the corrosion activation energy indicates that the extract is more effective in 1 M HCl at high temperatures and more effective at low temperatures in 0.5 M H_2SO_4.

DFT-based quantum chemical computations of parameters associated with the molecular electronic structures of the active constituents of the extract (paradol and shogaol) confirmed their corrosion inhibiting potential and established their individual contributions to the observed inhibiting effect. The non covalent adsorption geometries of both molecules on Fe show clear evidence of soft epitaxial adsorption and the magnitude of the physisorption energies agree more or less with the remarkable trend of experimentally determined inhibition efficiencies.

REFERENCES

[1] Desimone, M.P., Gordillo, G., and Simison, S.N. (2011) *Corros. Sci.*, 53: 4033–4043.
[2] Sadeghi Meresht, E., Shahrabi Farahani, T., and Neshati, J. (2012) *Corros. Sci.*, 54: 36–44.
[3] Zhang, D.-Q., Xie, B., Gao, L.-X., Cai, Q.-R., Joo, H.G., and Lee, K.Y. (2011) *Thin Solid Films*, 520: 356–361.
[4] Al-Sabagh, A.M., Elsabee, M., Elazabawy, O.E., and El-Tabey, A.E. (2010) *J. Dispersion Sci. Technol.*, 31: 1288–1297.
[5] Obi-Egbedi, N.O. and Obot, I.B. (2012) *Arabian J. Chem.*, 5: 121–133.
[6] Yang, X., Li, B., Wang, H., and Hou, B. (2011) *J. Dispersion Sci. Technol.*, 32: 672–676.
[7] Behpour, M., Ghoreishi, S.M., Khayatkashani, M., and Soltani, N. (2011) *Corros. Sci.*, 53: 2489–2501.
[8] Deng, S. and Li, X. (2012) *Corros. Sci.*, 55: 407–415.
[9] Ostovari, A., Hoseinieh, S.M., Peikari, M., Shadizadeh, S.R., and Hashemi, S.J. (2009) *Corros. Sci.*, 51: 1935–1949.
[10] Oguzie, E.E. and Onuchukwu, A.I. (2007) *Corrosion Reviews*, 25: 355–362.
[11] Satapathy, A.K., Gunasekaran, G., Sahoo, S.C., Amit, K., and Rodrigues, P.V. (2009) *Corros. Sci.*, 51: 2848–2856.
[12] Oguzie, E.E., Enenebeaku, C.K., Akalezi, C.O., Okoro, S.C., Ayuk, A.A., and Ejike, E.N. (2010) *J. Colloid Interface Sci.*, 349: 283–292.
[13] Doherty, V.F., Olaniran, O.O., and Kanife, U.C. (2010) *Int. J. Biol.*, 2: 126–131.
[14] Chung, W.Y., Jung, Y.J., Surh, Y.J., Lee, S.S., and Park, K.K. (2001) *Mutat. Res.*, 496: 199–206.
[15] Fernandez, X., Pintaric, C., Lizzani-Cuvelier, L., Loiseau, A-M., Morello, A., and Pellerin, P. (2005) *Flavour and Fragrance J.*, 21: 162–165.
[16] Popova, A., Sokolova, E., Raicheva, S., and Christov, M. (2003) *Corros. Sci.*, 45: 33–58.
[17] Ashassi-Sorkhabi, H., Seifzadeh, D., and Hosseini, M.G. (2008) *Corros. Sci.*, 50: 3363–3370.
[18] Oguzie, E.E., Li, Y., and Wang, F.H. (2007) *J. Colloid Interface Sci.*, 310: 90–98.
[19] Oguzie, E.E., Wang, S.G., Li, Y., and Wang, F.H. (2009) *J. Phys. Chem. C*, 113: 8420–8429.
[20] Abdel-Rahman, H.H. (2010) *J. Dispersion Sci. Technol.*, 31: 1740–1751.
[21] Villamil, R.F.V., Corio, P., Rubin, J.C., and Agostinho, S.M.L. (2002) *J. Electroanal. Chem.*, 535: 75–83.
[22] Ameer, M.A., Khamis, E., and Al-Senani, G. (2000) *Ads. Sci. Technol.*, 18: 177–193.
[23] Oguzie, E.E., Onuoha, G.N., and Onuchukwu, A.I. (2005) *Mater. Chem. Phys.*, 89: 305–311.
[24] Desimone, M.P., Gordillo, G., and Simison, S.N. (2011) *Corros. Sci.*, 53: 4033–4043.

[25] Delley, B.J. (1990) *Chem. Phys.*, 92: 508–518.
[26] Delley, B.J. (2000) *Chem. Phys.*, 113: 7756–7765.
[27] Tang, Y., Yao, L., Kong, C., Yang, W., and Chen, Y. (2011) *Corros. Sci.*, 53: 2046–2049.
[28] Khaled, K.F. (2010) *Corros. Sci.*, 52: 2905–2916.
[29] Obot, I.B. and Obi-Egbedi, N.O. (2010) *Corr. Sci.*, 52: 198–204.
[30] Gece, G. (2008) *Corros. Sci.*, 52: 2981–2992.
[31] Cruz, J., Pandiyan, T., and Garcıa-Ochoa, E. (2005) *J. Electroanal. Chem.*, 583: 8–16.
[32] Fu, J., Li, S., Wang, Y., Cao, L., and Lu, L. (2010) *J. Mater. Sci.*, 45: 6255–6265.
[33] Casewit, C.J., Colwell, K.S., and Rappé, A.K. (1992) *J. Am. Chem. Soc.*, 114: 10035–10046.
[34] Casewit, C.J., Colwell, K.S., and Rappé, A.K. (1992) *J. Am. Chem. Soc.*, 114: 10046–10053.
[35] Feng, J., Pandey, R.B., Berry, R.J., Farmer, B.L., Naik, R.R., and Heinz, H. (2011) *Soft Matter*, 7: 2113–2120.
[36] Heinz, H., Farmer, B.L., Pandey, R.B., Slocik, J.M., Patnaik, S.S., Pachter, R., and Naik, R.R. (2009) *J. Am. Chem. Soc.*, 131: 9704–9714.
[37] Chidiebere, M.A., Ogukwe, C.E., Oguzie, K.L., Eneh, C.N., and Oguzie, E.E. (2012) *Ind. Eng. Chem. Res.*, 51: 668–677
[38] Mejeha, I.M., Nwandu, M.C., Okeoma, K.B., Nnanna, L.A., Chidiebere, M.A., Eze, F.C., and Oguzie, E.E. (2012) *J. Mater. Sci.*, 47: 2559–2572.